

Composition Dependence of the Charge Driven Phase Transition in Group-VI Transition Metal Dichalcogenides

Urvesh Patil and Nuala M. Caffrey*

School of Physics and CRANN, Trinity College, Dublin 2, Ireland

E-mail: nuala.caffrey@tcd.ie

December 20, 2024

Abstract

Materials exhibiting multiple stable phases can be used as functional components in electronic and optical applications if the phase transition is controllable. Group-VI transition metal dichalcogenides (TMDs, MX_2 , where $M=Mo, W$ and $X = S, Se$) are known to undergo charge induced transitions from semi-conducting H phases to metallic T phases. However, it is difficult to experimentally decouple the effect of composition-dependent energy barriers from indirect effects related to alkali metal-induced exfoliation. Here, using first-principles calculations, we study the energetics of transition between the different structural polytypes of four group-VI TMDs upon lithium adsorption. The calculated barriers provide an explanation for the high proportion of H phase remaining in alkali-treated MoS_2 compared to other group-VI monolayers. Likewise, the high proportion of metallic phase in WS_2 monolayers after alkali treatment can be explained by a high barrier to revert back to the H phase once in a neutral state.

Transition metal dichalcogenides (TMDs), comprised of layered sheets of transition metal atoms sandwiched between two layers of chalcogen atoms (MX_2), are chemically versatile, exhibiting a broad range of electronic properties from insulating (ZrS_2) to superconducting ($NbSe_2$).¹ As well as by changing the composition, the conductivity of a TMD can be modified by inducing a structural transition between different polymorphs. Several such polymorphs exist, distinguished by the metal coordination of the chalcogen atoms. In the semi-conducting H phase, the chalcogen atoms are AA-stacked so that the metal atoms occupy alternate trigonal-prismatic voids. The metallic T phase, on the other hand, has a tetragonal symmetry, with the metal atoms occupying octahedral voids between AB-stacked chalcogen atoms. This particular phase can transform to a semi-metallic distorted octahedral phase, designated here T'. Recently, a further phase, designated T'', which can be viewed as a series of alternating H and T' phases, was predicted to be lower in energy than the T' phase for MoS_2 .²

Whether a particular TMD has a hexagonal, tetragonal or mixed phase ground state depends on its d -electron count.^{3,4} For example, group-IV TMDs (such as TiS_2 and ZrS_2) and group-VI TMDs (such as MoS_2 and WSe_2) typically exhibit the T phase and H phase respectively, while group-V TMDs (such as NbS_2 and $TaSe_2$) have both H and T ground states. This suggests a route towards the control of the TMD phase via the manipulation of the d electron count. This could be achieved, for example, by inducing charge transfer from a reducing agent to the TMD. Indeed, the ability to induce a transition in MoS_2 from its ground state H phase to an octahedral phase via alkali metal intercalation has been known since the 1980s.⁵ This phase transition was attributed to a transfer of charge from the intercalated atom to the TMD, and more specifically to the d states of the transition metal atom. Indeed, the entire family of group-VI TMDs, where $M = Mo, W$ and $X = S, Se$ and Te, can be manipulated to undergo phase transitions close to ambient conditions.⁶ This has been achieved using a variety of methods, including alkali metal adsorption,^{5,7–9} the introduction of impurities or vacancies,^{10–12} electron or laser irradiation^{11,13–17} and electrostatic gating.^{18,19}

The electronic properties of a TMD are evidently strongly dependent on its structural phase. In MoS_2 the conductivity of the T phase was found to be up to 10^7 times higher than that of the semiconducting H phase.²⁰ The ability to reversibly and reliably switch between these two phases would result in applications as monolayer-thick field effect transistors,²¹ gas sensors²² and catalysts.²³ Such applications require precise control over the phase transition process.

Of the group-VI TMDs, the phase transition in MoS_2 has been investigated in detail. Yet, compared to other group-VI TMDs, the phase transition efficiency in MoS_2 is relatively low: a comprehensive side-by-side comparison of the experimental transition efficiency in four group-VI TMDs – MoS_2 , $MoSe_2$, WS_2 and WSe_2 – found that WS_2 exhibited the largest increase in the

proportion of the 1T phase compared to the starting 2H phase (i.e., the 1T/2H ratio), followed by MoSe_2 and WSe_2 , and eventually MoS_2 .²⁴ While the exact T/H ratio was subsequently found to depend on the nature of the organolithium intercalant group used in the experiment, the general trend remained: WX_2 compounds display a higher proportion of T phase compared to MoX_2 , for both $\text{X} = \text{S}$ and Se .^{25,26}

In such experiments, alkali metal atoms are used to simultaneously exfoliate the bulk TMD and to induce the phase transition. As a result, the measured phase transition efficiency depends not only on the intrinsic composition-dependent free-energy barrier between the different phases, but also on the composition-dependent exfoliation efficiency of the chosen organolithium intercalant. Experimentally, it is difficult to decouple the two contributions.

Previous computational investigations of the phase transition barrier have also concentrated on MoS_2 , looking primarily at the threshold charge density required to induce the phase transition. However, a disconcertingly wide range of values have been reported, including 0.35 e per formula unit (f.u.),²⁷ 0.55 e per f.u.,² 0.78 e per f.u.²⁸ and almost 2 e per f.u.²⁹

Here, using first-principle calculations, we determine the transition barriers between all possible polytypes of both the pristine and Li-adsorbed group-IV TMDs, with the aim of determining whether the experimental results in the literature can be explained using the intrinsic barriers to the phase transitions alone. We also discuss some issues related to statically charging the unit cell in density functional theory and show that the majority of results obtained using such methods are incorrect.

The crystal structures of the H, T' and T'' phases are shown in Fig. 1 and the geometrically optimized lattice parameters for each of the considered materials in these phases are given in Table 1. The lattice constants are

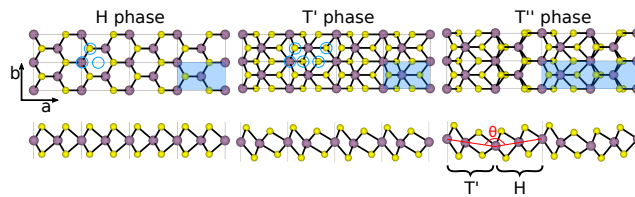


Figure 1: Top and side view of the H, T' and T'' polytypes. The orthorhombic cells of all three phases are shown as blue shaded regions. Note that the T'' phase can be viewed as alternating T' and H phases. The angle formed between the planes of the metal atoms of these two phases, $M_H - M_H$ and $M_{T'} - M_{T'}$, is defined as the dihedral angle, θ . The blue circles indicate the possible candidate sites for lithium adsorption.

dictated by the chalcogen atom, with MoS_2 and WS_2 having very similar values in all three phases. Likewise, MoSe_2 and WSe_2 have almost identical lattice constants. In the case of the T'' phase, the dihedral angle between the planes of metal atoms is almost identical for all four

materials, at approximately 179 degrees. These values are in good agreement with the available experimental data³⁹⁻⁴⁸ and with previous calculations⁴⁹⁻⁵² in the literature. For the T' phase, the calculated a lattice constant of 5.57 Å for MoS_2 is consistent with the experimentally observed length of 5.6 Å.⁵³

Table 1: The lattice parameters a , b (in Å) of the H, T', and T'' phases of MoS_2 , MoSe_2 , WS_2 and WSe_2 .

	H		T'		T''	
	a	b	a	b	a	b
MoS_2	5.48	3.16	5.57	3.22	11.23	3.16
MoSe_2	5.71	3.30	5.79	3.34	11.69	3.27
WS_2	5.48	3.17	5.59	3.23	11.24	3.18
WSe_2	5.71	3.30	5.81	3.35	11.69	3.28

In agreement with previous DFT studies, we find the H phase to be the ground state structure for all four materials.^{11,19,28,29,54-56} The total energy differences between this phase and both the T' and the T'' phases are given in Fig. 2. We find that the energy differ-

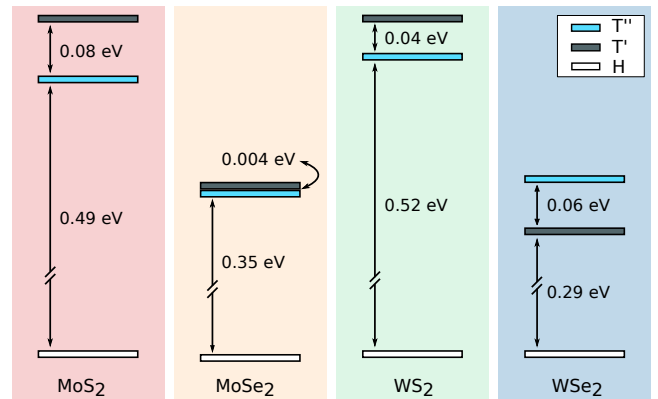


Figure 2: The relative energies of the T' and T'' phases compared to the H phase for MoS_2 , MoSe_2 , WS_2 and WSe_2 .

ence between the H phase and the T' phase is larger for the sulphides compared to the selenides. It reduces from 0.57 eV for MoS_2 to 0.35 eV for MoSe_2 and from 0.56 eV for WS_2 to 0.29 eV for WSe_2 . Similarly, the energy difference between the H phase and the T'' phase reduces from 0.49 eV for MoS_2 to 0.35 eV for MoSe_2 and from 0.52 eV for WS_2 to 0.35 eV for WSe_2 . While the H phase is the ground state in all four cases, it is notable that the T' phase is energetically more favourable than the T'' phase for WSe_2 but the ordering is opposite for the other three materials (although the difference is negligible for MoSe_2).

The band structures of these materials in all three phases are shown in Fig. 3. The opening of a band-gap in the H phase is due to a mixing of the p_z orbitals

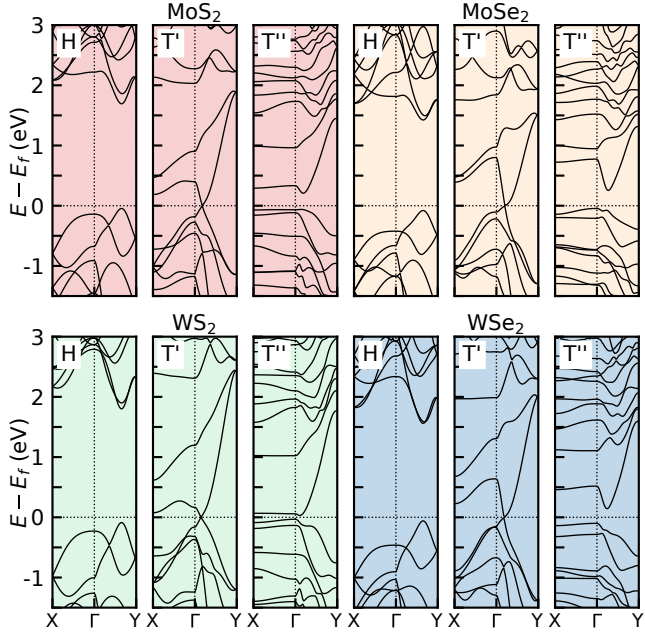


Figure 3: The band structure of the H, T' and T'' phases of MoS₂, MoSe₂, WS₂ and WSe₂.

from the top and bottom chalcogen atoms at K-point of the hexagonal Brillouin zone.³ We find a bandgap of 1.74, 1.50, 1.90 and 1.62 eV for MoS₂, MoSe₂, WS₂ and WSe₂, respectively, in good agreement with previous calculations in the literature.^{57,58} The band gaps for the MSe₂ compounds are smaller compared to the corresponding MS₂ compounds. As a result of the AB-type stacking of the chalcogen atoms in the T phase, this particular p_z interlayer mixing is absent, and the bandgap closes. The distortion of the T phase to produce the T' phase facilitates in part this interaction again, so that the resulting phase is semimetallic³ (The inclusion of spin-orbit coupling opens a small band gap.⁵⁹) The relative energy ordering of the H and the T' phase is driven by this interlayer interaction.

The alternating H (insulating) and T' (metallic) stripes in the T'' phase (cf. Fig. 1) produces an effective one-dimensional (1D) quantum well structure, with flat bands evident perpendicular to the direction of confinement (here, along Γ – X). This confinement causes the overlapping energy levels in the T' phase to split, opening a small band-gap of 0.27, 0.29, 0.05 and 0.25 eV for MoS₂, MoSe₂, WS₂ and WSe₂, respectively, in good agreement with the previous calculations of Ma et al.² The formation of these 1D quantum wells causes the T'' phase to be lower in energy than the T' phase for MoS₂, MoSe₂ and WS₂.

The activation barriers to induce a phase transition from the H phase to the T' and T'' phases, as calculated with the CI-NEB method, for all four materials are shown in Fig. 4. In all cases, the energy barrier to transition directly from the H phase to the T' phase is large, ranging between 1.22 eV and 1.54 eV. In general, the barrier is smaller for MSe₂ than for MS₂. The energy

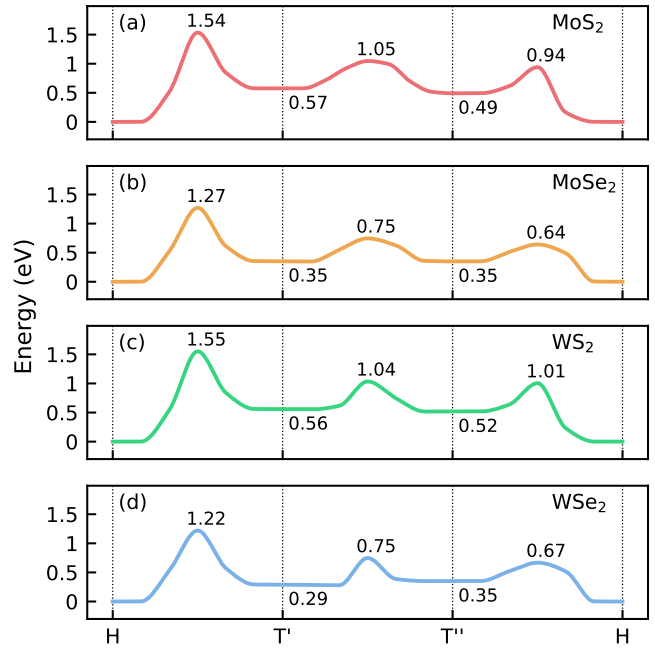


Figure 4: The relative energy difference and transition barrier between the H phase, the T' phase and the T'' phase of (a) MoS₂, (b) MoSe₂, (c) WS₂ and (d) WSe₂. Energies are referred that of the H phase for each material.

barrier to transition from the H phase to the T'' phase is smaller, ranging between 0.64 eV and 1.01 eV. Again, the smallest values occur for the MSe₂ compounds. Finally, the barrier to transition from the T' phase to the T'' phase is 0.48 eV for both MoS₂ and WS₂, whereas it is 0.40 eV and 0.46 eV for MoSe₂ and WSe₂, respectively. Note that the transition from the T' phase to the T'' phase requires the conversion of only half of the lattice from the T' phase to the H phase while keeping the other half fixed. Consequently, the barrier to transition from the T' phase to the T'' phase is lower (by between 50 and 65%) than the barrier to undergo the complete transition from T' phase to the H phase.

In all cases the energy barrier to transition from the ground state H phase to the lowest-lying T phase (namely, T'' for MoS₂, MoSe₂ and WS₂, and T' for WSe₂) lies between 0.64 eV and 1.22 eV. Evidently, the H phase is very stable and will not convert to the T phase spontaneously, in agreement with experiment.

Before discussing the effects of Li adsorption on the energy barriers to the phase transition, we first highlight some issues related to statically charging monolayers or slabs in DFT with periodic boundary conditions. Clearly, repeating charged monolayers will have a divergent electric potential energy. To compensate for this, a correction is typically added to the potential, or equivalently a neutralizing background charge is applied. When this method is applied to two dimensional slabs in a vacuum, several issues arise which are typically overlooked. These are briefly summarized below:

For the case of isolated charged slabs, such as the

TMD monolayers considered here, the electric field due to the extra uniform charge density is constant and should result in potential that varies linearly with distance from the surface of the slab. When periodic boundary conditions are implemented, this linear potential is replaced by the combined effective potential due to the consecutive periodic images. The quantities relating to the isolated slabs can be recovered from these periodic calculations by applying a correction term to the effective potential and total energy. The exact functional form of this potential is discussed in detail by Andreussi et al.⁶⁰ In VASP the leading term of this correction, which cancels the interaction of the linear potential with the background compensating charge, is absent. As a result, the total energy is essentially incorrect and cannot be relied upon.

Furthermore, we find that above a certain critical charge, positive eigenvalues are occupied. This was previously shown to occur for atomic anions and can be attributed to the self-interaction error.⁶¹

Finally, Topsakal et al. showed that, when the basis set covers the vacuum region, beyond a critical value which depends in the vacuum thickness, excess negative charge does not stay on the slab but spills over in the vacuum.⁶² This phenomenon is demonstrated in Fig. 5(a) for the H phase of MoS₂ with a vacuum length of 25 Å perpendicular to the surface of the slab and was previously shown for graphene.⁶³ The excess charge density added is placed on the vacuum and on the outer faces of the monolayer rather than on the *d* orbital of the metal atom.

It is to these issues that we attribute the wide range of values reported in the literature for the critical charge required to induce a structural phase transition in TMDs. To illustrate this, we show in Fig. 5(b) the total energy difference between the H and the T' phase of MoS₂ as a function of excess charge, and for two different vacuum lengths. In this case all three sources of error are present, namely charge has spilled into the vacuum (above a certain critical excess charge value), the appropriate monopole correction is absent and positive eigenvalues are occupied. We find that the vacuum length of 15 Å (blue) shows a phase transition for excess charge of around 0.5 e per f.u. On increasing the vacuum length to 25 Å (orange) no such transition is observed. This system dependence of the calculations are also reported by Bal et al. for adsorbed molecules on charged surfaces and highlight the irreproducibility of such results.⁶⁴

Introducing extra charge to the TMD via an interaction with strong donor atoms bypasses these issues. We consider two different concentrations of Li atoms adsorbed on the surface of the monolayers, namely Li_{0.5}MX₂ and Li₁MX₂. The stability of the alkali metal adsorbed monolayer decreases at higher concentrations, and eventually becomes unstable for Li_{1.5}MX₂, in agreement with experiment.^{53,65,66}

The adsorption sites were determined by calculating the total energy of lithium adsorbed on all of the unique

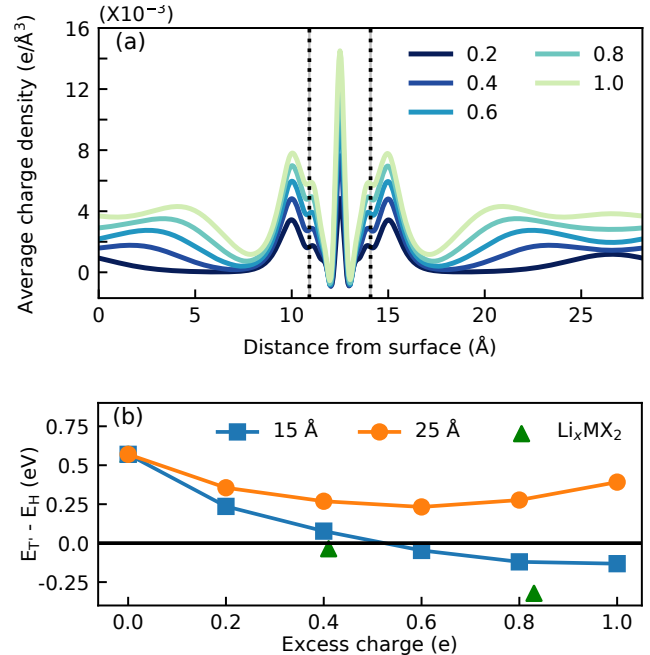


Figure 5: (a) Planar average of the charge density across the TMD monolayers showing charge leakage into the vacuum region for typical values of excess charge. The positions of the chalcogen atoms are marked by black dashed lines. (b) The energy difference between the T' and the H phase of MoS₂ as a function of excess static charge for two different vacuum thickness, compared to the values found by explicitly charging the slab using Li atoms.

candidate sites, shown as blue dots in Fig. 1. These sites include directly on top of the metal atom, on top of the chalcogen atoms and on the hollow site. Irrespective of the material or phase, we find the lowest energy adsorption site to be on top of the metal atom, in agreement with previous calculations in the literature.⁶⁷ When increasing the Li concentration to LiMX₂, the second Li atom per unit cell adsorbs on the opposite surface, minimizing the electrostatic interaction between the two Li atoms. This configuration is 0.1 eV lower in energy than that with both Li atoms adsorbed on the same side of the monolayer. For the case of the T'' phase, the lithium atoms are also positioned on top of the metal atoms. For Li_{0.5}MX₂, one lithium atom is placed in the H phase region and another in the T' phase region. For Li₁MX₂, the next lithium atom was placed on top the remaining metal atoms on the opposite side of the slab.

The extra charge introduced by the Li atoms causes an expansion of the TMD lattice constants. These values are given in Table 2. A Li concentration of Li_{0.5}MX₂ increases the lattice constants of the H phase by between 0.9 and 1.8% compared to the neutral lattice. Similarly, Li adsorption increases the lattice constants of the T' phase by between 1.8% and 2.7%. Increasing the lithium concentration causes the lattice to expand further, and the expansion is higher in the selenides compared to the sulfides.

Table 2: The lattice parameters a , b (in Å) of the H, T' and T'' phase of $\text{Li}_{0.5}\text{MX}_2$ and LiMX_2 in the orthorhombic unit cell.

Å	$\text{Li}_{0.5}\text{MX}_2$						LiMX_2					
	H		T'		T''		H		T'		T''	
	a	b	a	b	a	b	a	b	a	b	a	b
MoS_2	5.58	3.22	5.69	3.28	11.49	3.20	5.61	3.24	5.77	3.33	11.79	3.22
MoSe_2	5.81	3.36	5.94	3.43	11.95	3.34	5.89	3.40	6.09	3.52	12.2	3.38
WS_2	5.55	3.20	5.71	3.29	11.47	3.19	5.58	3.22	5.79	3.34	11.72	3.19
WSe_2	5.80	3.35	5.95	3.44	11.90	3.33	5.84	3.37	6.08	3.51	12.30	3.33

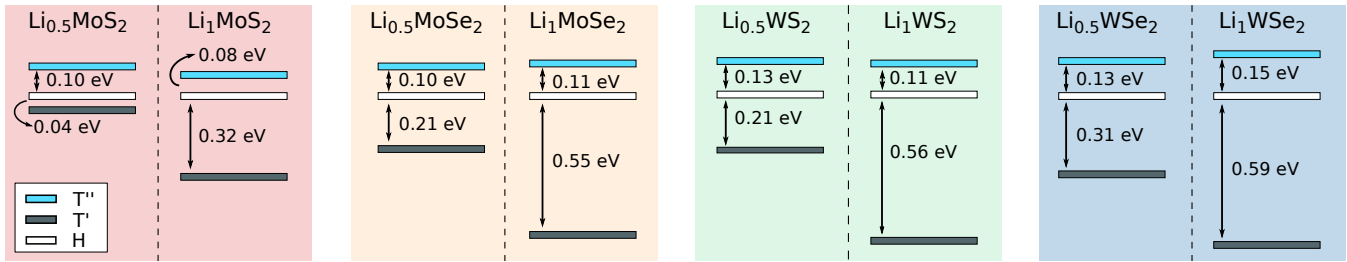


Figure 6: Relative energies of the T' and T'' phases compared to the H phase of Li_xMoS_2 , Li_xMoSe_2 , Li_xWS_2 and Li_xWSe_2 with $x = 0.5$ and 1. All figures are aligned using the energy of the H phase.

Bader charge analysis⁶⁸ finds that, for both concentrations considered here, each Li atom donates approximately 0.82 electrons per formula unit. This value is independent of the material type and phase, indicating that the nature of the interaction is similar. The adsorption energies, defined as $E_{\text{ads}} = E_{\text{Li}_x\text{MX}_2} - E_{\text{MX}_2} - xE_{\text{Li}}$ where $E_{\text{Li}_x\text{MX}_2}$ is the total energy of the Li adsorbed structure, $E_{\text{Li}_x\text{MX}_2}$ is the total energy of the pristine monolayer, E_{Li} is the energy of an isolated Li atom and x refers to the Li concentration, for all four materials are given in Table 3. Li adsorbed on MoS_2 has the highest adsorption energy, irrespective of the phase. The Li adsorption energy is higher for T' phase as compared to the H phase. On increasing the lithium concentration from $\text{Li}_{0.5}\text{MX}_2$ to LiMX_2 , the adsorption energy more than doubles for H phase but is slightly small than double for the T' phase.

Table 3: Lithium adsorption energy on the H and T' phase per unit MX_2 .

	$\text{Li}_{0.5}\text{MX}_2$		LiMX_2	
	$E_{\text{ads}}^{\text{H}}$	$E_{\text{ads}}^{\text{T}'}$	$E_{\text{ads}}^{\text{H}}$	$E_{\text{ads}}^{\text{T}'}$
MoS_2	-0.92	-1.53	-2.07	-2.96
MoSe_2	-0.85	-1.42	-1.91	-2.81
WS_2	-0.81	-1.58	-1.83	-2.95
WSe_2	-0.77	-1.37	-1.73	-2.61

The energy differences between the different poly-

types, for all four compounds and for both Li concentrations, are summarized in Fig. 6. The T' phase becomes the ground state structure of all four Li-adsorbed TMDs. This is followed by the H phase and finally the T'' phase. This is in agreement with previous studies on MoS_2 which have shown a phase transition to occur at a Li concentration of $\text{Li}_{0.4}\text{MoS}_2$,⁶⁹ a K concentration of $\text{K}_{0.225}\text{WSe}_2$ ⁹ and a Na concentration of $\text{Na}_{0.375}\text{MoS}_2$.⁶⁵

The energy difference between both the T' and T'' phases compared to the H phase increases going down the group from S to Se and also going from Mo to W for both considered Li concentrations. On increasing the lithium concentration from $\text{Li}_{0.5}\text{MX}_2$ to Li_1MX_2 , the energy difference between the T'' phase and the H phase decreases slightly for the sulfides but increases for the selenides. The energy difference between T'' and the H phase decreases from 0.10 eV to 0.08 eV for MoS_2 and from 0.13 eV to 0.11 eV for WS_2 , whereas it increases from 0.10 eV to 0.11 eV for MoSe_2 and from 0.13 eV to 0.15 eV for WSe_2 . In contrast to our observation that the energy of the T'' phase increases with respect to the H phase, Ma et al. reported a threshold of 0.4 e per MoS_2 for transition from H to T'' phase.² This discrepancy could be a consequence of the static charging method used in obtaining those results.

These trends in stability can be explained by simple electron filling in the rigid band approximation.⁹ For the H and T'' phases, excess electrons cause an increase in total energy equal to the band gap. As the T' phase is semi-metallic, the next available energy level is at the Fermi level, and so this phase becomes lower in energy.

The barriers for the H to T' phase transition in the

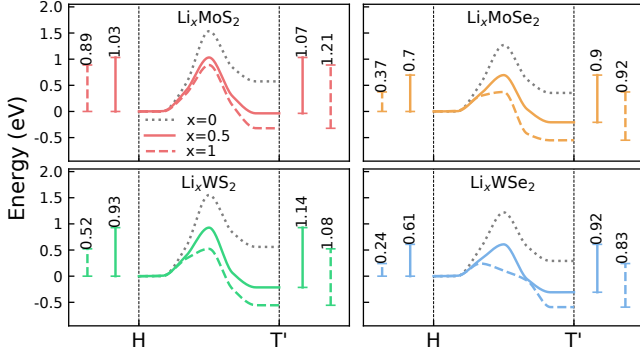


Figure 7: The relative energy difference and transition barrier between the H phase and the T' phase of Li_xMoS_2 , Li_xMoSe_2 , Li_xWS_2 and Li_xWSe_2 with $x = 0$ (dotted line), $x = 0.5$ (solid line) and $x = 1$ (dashed line). Energies are referred to that of the H phase of each material.

charged monolayers are shown in Fig. 7. In all cases, the barrier for the phase transition decreases due to lithium adsorption. The maximum barrier for the transition from the H phase to the T' phase is found for MoS_2 at a value of 1.03 eV for $\text{Li}_{0.5}\text{MX}_2$ and 0.89 eV for $\text{Li}_{0.5}\text{MX}_2$. The minimum transition barrier from the H phase to the T' phase is found for WSe_2 with a barrier of 0.61 eV for $\text{Li}_{0.5}\text{MX}_2$ and 0.24 eV for Li_1MX_2 . WS_2 has the second highest barrier, at a value of 0.5 eV for the Li_1MX_2 structure, while MoSe_2 has a barrier of 0.37 eV at the same Li concentration. In all cases, the barrier to transition does not decrease to zero. As such, the transition cannot be spontaneous and an energy equal to the barrier height needs to be provided to induce the transition.

We note however that Li adsorption is an exothermic process. For $\text{Li}_{0.5}\text{MX}_2$, the adsorption energy is largest for the two MoX_2 materials, at approximately -0.9 eV and slightly smaller for WX_2 at -0.8 eV. This energy is comparable to the energy barrier to the phase transition at this Li concentration. For Li_1MX_2 , the adsorption energy per MX_2 approximately doubles, to at least 2.5 times the energy barrier. If some of this energy is used to overcome the barrier to the transition, Li adsorption may be sufficient to make the process spontaneous. Furthermore, given that the rate of transition decreases exponentially with activation energy (as per the Arrhenius equation), we can conclude that, for a given X, WX_2 will transition at a higher rate than MoX_2 . Likewise, for a given M, MSe_2 will transition at a higher rate than MS_2 .

While this can explain the relatively poor experimental transition of MoS_2 (the energy barrier is still high at 0.89 eV even at a Li concentration of Li_1MoS_2), it does not explain the much higher percentage of T' phase found for WS_2 compared to MoSe_2 and WSe_2 . To explain this, we must also consider the fact that in order to measure the T/H ratio experimentally, the exfoliated monolayers are washed with deionized water and dried in vacuum. In this process the Li ions desorb and

the monolayers revert to their neutral state. This is supported by the observation of the M(IV) rather than M(VI) oxidation state in X-ray photo electron spectra (XPS).^{24,25,65} The monolayers have transitioned to the T' phase but are prevented from transitioning immediately back to the ground-state H phase by an energy barrier.

The neutral barriers shown in Fig. 4 are now relevant. For all materials, the barrier to return directly to the H phase is prohibitively high, ranging between 0.90 eV and 0.99 eV. Instead, the barrier to transition to the T'' phase is significantly lower, ranging between 0.39 eV and 0.48 eV. The subsequent barrier to transition from the T'' phase to the H phase is small for the two selenium compounds at 0.23 eV and 0.27 eV for MoSe_2 and WSe_2 , respectively. The barrier for WS_2 is twice as high, at 0.49 eV. The significance of this difference in barrier for WS_2 and WSe_2 can be determined by calculating the exponential factor of the Arrhenius equation at room temperature ($k_B T = 25.7$ meV). It is of the order of 5×10^{-9} for WS_2 , whereas it is of the order of 1×10^{-4} for WSe_2 . This rate difference is significant and its effects should be experimentally observable.

Experimental evidence for such an indirect transition from the T' phase back to the H phase for MoS_2 via a T'' phase exists: By fitting the rate equation to in-situ Raman measurements the barrier to transform from the meta-stable metallic phase to the ground state was found to be 400 meV.¹⁷ This barrier value is consistent with the calculated transition from T'' phase to H phase of 450 meV calculated here (cf. Fig. 4) whereas the barrier to transition from the T' phase back to the H phase directly is 970 meV. This suggests that the transition from the T' phase to the H phase occurs in two steps for this material, via the T'' phase.

Finally, we note that the T'' phase, which is comprised of alternating H and T' phases each a unit cell thick, can be viewed as just one example of a family of mixed T' and H phase structures. By changing the T':H ratio in MoS_2 from 1:1 for the T'' structure to 2:1, the total energy difference between it and the H phase increases from 0.49 eV to 0.51 eV. By increasing the ratio further to 3:1, the energy difference increases further to 0.52 eV. Clearly, the total energy of MoS_2 is strongly dependent upon the fraction of H phase. The energy of all such families of confined structures will be higher than that of the H phase but lower than that of the T' phase. The exact composition of such confined structures will be dependent on the available energy and the TMD flake size and shape and are not confined to the one dimensional structures discussed here. The final structures observed experimentally are found to vary from no phase transition to a partial phase transition with island formation. These islands are observed to have atomically sharp boundaries between the H phase and the T' phase areas which evolve over time via a transversal displacement of one of the S planes¹³ leading to the complete phase transition of the flake. The observed partial phases, with mixed metallic (T') and

insulating (H) regions, can be understood as intermediate stable structures which have lower barriers of transition.

In conclusion, we show that the experimentally-reported relative difficulty in converting the H phase of MoS_2 to the T' phase can be explained by a higher barrier for the charge-induced transition in this material compared to the others. Increasing the concentration of adsorbed Li does not decrease this barrier significantly. In contrast, while the barrier of neutral WS_2 is very similar to that of MoS_2 , it reduces significantly at higher Li concentrations. Once in the T' phase, and in a neutral state, as it would be in the experiment, there is a larger barrier for WS_2 to revert back to the H phase compared to MoSe_2 and WSe_2 . In general, the ratio of T' to H phase is maximized if the charge-induced transition from the H phase to the T' phase is favourable and the reverse transition upon removal of charge is unfavorable. When applied to the group-VI TMDs, this can explain the general trend that WX_2 compounds display a higher proportion of T phase compared to MoX_2 after alkali metal intercalation, for both X = S and Se.

Computational Methods

Density functional theory (DFT) calculations are performed using the VASP-5.4 code.^{30–32} The optB86b-vdW exchange-correlation functional was used to account for long range dispersion interactions.^{33,34} This functional was previously shown to give accurate lattice parameters and energies for layered materials^{35,36}. All calculations are performed with a cutoff energy of 500 eV for the plane wave basis set. A Γ centered K-point grid of $11 \times 7 \times 1$ is used to calculate the total energy of the H and T' phases, while a $11 \times 5 \times 1$ grid is used for the T'' phase.

The structures are relaxed until the force on each atom is less than 0.01 eV/Å. The unit cell length in the direction normal to the plane is fixed at 25 Å for H and T' phase calculations, and 26 Å for T'' phase calculations and all transition state calculations. This corresponds to a minimum vacuum of 18 Å between repeating monolayers and the dipole corrections are applied.

Transition states are determined using the climbing image nudged elastic band (CI-NEB) method^{37,38} with a spring constant of 5. All atoms in the transition state calculations are optimized so that the force on each atom is less than 0.01 eV/Å.

Acknowledgement This work was supported by a Science Foundation Ireland Starting Investigator Research Grant (15/SIRG/3314). Computational resources were provided by the supercomputer facilities at the Trinity Center for High Performance Computing (TCHPC) and at the Irish Center for High-End Computing (project tcphy091b).

References

- (1) Manzeli, S.; Ovchinnikov, D.; Pasquier, D.; Yazyev, O. V.; Kis, A. 2D transition metal dichalcogenides. *Nature Reviews Materials* **2017**, *2*, 17033.
- (2) Ma, F.; Gao, G.; Jiao, Y.; Gu, Y.; Bilic, A.; Zhang, H.; Chen, Z.; Du, A. Predicting a new phase (T'') of two-dimensional transition metal di-chalcogenides and strain-controlled topological phase transition. *Nanoscale* **2016**, *8*, 4969–4975.
- (3) Kertesz, M.; Hoffmann, R. Octahedral vs. trigonal-prismatic coordination and clustering in transition-metal dichalcogenides. *Journal of the American Chemical Society* **1984**, *106*, 3453.
- (4) Chia, X.; Pumera, M. Layered transition metal dichalcogenide electrochemistry: journey across the periodic table. *Chemical Society Reviews* **2018**,
- (5) Py, M.; Haering, R. Structural destabilization induced by lithium intercalation in MoS_2 and related compounds. *Canadian Journal of Physics* **1983**, *61*, 76–84.
- (6) Voiry, D.; Mohite, A.; Chhowalla, M. Phase engineering of transition metal dichalcogenides. *Chemical Society Reviews* **2015**, *44*, 2702.
- (7) Gamble, F. Ionicity, atomic radii, and structure in the layered dichalcogenides of group IVb, Vb, and VIb transition metals. *Journal of Solid State Chemistry* **1974**, *9*, 358–367.
- (8) Wang, L.; Xu, Z.; Wang, W.; Bai, X. Atomic mechanism of dynamic electrochemical lithiation processes of MoS_2 nanosheets. *Journal of the American Chemical Society* **2014**, *136*, 6693–6697.
- (9) Lei, B.; Pan, Y.; Hu, Z.; Zhang, J.; Xiang, D.; Zheng, Y.; Guo, R.; Han, C.; Wang, L.; Lu, J. et al. Direct Observation of Semiconductor–Metal Phase Transition in Bilayer Tungsten Diselenide Induced by Potassium Surface Functionalization. *ACS nano* **2018**, *12*, 2070–2077.
- (10) Raffone, F.; Ataca, C.; Grossman, J. C.; Cicero, G. MoS_2 enhanced T-phase stabilization and tunability through alloying. *The journal of physical chemistry letters* **2016**, *7*, 2304–2309.
- (11) Kretschmer, S.; Komsa, H.-P.; Bøggild, P.; Krasheninnikov, A. V. Structural Transformations in Two-Dimensional Transition-Metal Dichalcogenide MoS_2 under an Electron Beam: Insights from First-Principles Calculations. *The Journal of Physical Chemistry Letters* **2017**, *8*, 3061–3067.

(12) Pizzochero, M.; Yazeyev, O. V. Point defects in the 1 T and 2 H phases of single-layer MoS₂: A comparative first-principles study. *Physical Review B* **2017**, *96*, 245402.

(13) Lin, Y.-C.; Dumcenco, D. O.; Huang, Y.-S.; Suenaga, K. Atomic mechanism of the semiconducting-to-metallic phase transition in single-layered MoS₂. *Nature nanotechnology* **2014**, *9*, 391.

(14) Cho, S.; Kim, S.; Kim, J. H.; Zhao, J.; Seok, J.; Keum, D. H.; Baik, J.; Choe, D.-H.; Chang, K. J.; Suenaga, K. et al. Phase patterning for ohmic homojunction contact in MoTe₂. *Science* **2015**, *349*, 625–628.

(15) Kang, Y.; Najmaei, S.; Liu, Z.; Bao, Y.; Wang, Y.; Zhu, X.; Halas, N. J.; Nordlander, P.; Ajayan, P. M.; Lou, J. et al. Plasmonic hot electron induced structural phase transition in a MoS₂ monolayer. *Advanced Materials* **2014**, *26*, 6467–6471.

(16) Fan, X.; Xu, P.; Zhou, D.; Sun, Y.; Li, Y. C.; Nguyen, M. A. T.; Terrones, M.; Mallouk, T. E. Fast and efficient preparation of exfoliated 2H MoS₂ nanosheets by sonication-assisted lithium intercalation and infrared laser-induced 1T to 2H phase reversion. *Nano letters* **2015**, *15*, 5956–5960.

(17) Guo, Y.; Sun, D.; Ouyang, B.; Raja, A.; Song, J.; Heinz, T. F.; Brus, L. E. Probing the dynamics of the metallic-to-semiconducting structural phase transformation in MoS₂ crystals. *Nano letters* **2015**, *15*, 5081–5088.

(18) Radisavljevic, B.; Kis, A. Mobility engineering and a metal–insulator transition in monolayer MoS₂. *Nature materials* **2013**, *12*, 815.

(19) Wang, Y.; Xiao, J.; Zhu, H.; Li, Y.; Alsaied, Y.; Fong, K. Y.; Zhou, Y.; Wang, S.; Shi, W.; Wang, Y. et al. Structural phase transition in monolayer MoTe₂ driven by electrostatic doping. *Nature* **2017**, *550*, 487.

(20) Acerce, M.; Voiry, D.; Chhowalla, M. Metallic 1T phase MoS₂ nanosheets as supercapacitor electrode materials. *Nature nanotechnology* **2015**, *10*, 313.

(21) Nourbakhsh, A.; Zubair, A.; Sajjad, R. N.; Tavakkoli KG, A.; Chen, W.; Fang, S.; Ling, X.; Kong, J.; Dresselhaus, M. S.; Kaxiras, E. et al. MoS₂ field-effect transistor with sub-10 nm channel length. *Nano letters* **2016**, *16*, 7798–7806.

(22) Friedman, A. L.; Perkins, F. K.; Hanbicki, A. T.; Culbertson, J. C.; Campbell, P. M. Dynamics of chemical vapor sensing with MoS₂ using 1T/2H phase contacts/channel. *Nanoscale* **2016**, *8*, 11445–11453.

(23) Luxa, J.; Vosecký, P.; Mazáček, V.; Sedmidubský, D.; Pumera, M.; Sofer, Z. Cation-Controlled Electrocatalytical Activity of Transition-Metal Disulfides. *ACS Catalysis* **2018**, *8*, 2774–2781.

(24) Ambrosi, A.; Sofer, Z.; Pumera, M. 2H $\xrightarrow{\text{H}_2}$ 1T phase transition and hydrogen evolution activity of MoS₂, MoSe₂, WS₂ and WSe₂ strongly depends on the MX₂ composition. *Chemical Communications* **2015**, *51*, 8450–8453.

(25) Rohaizad, N.; Mayorga-Martinez, C. C.; Sofer, Z.; Pumera, M. 1T-Phase Transition Metal Dichalcogenides (MoS₂, MoSe₂, WS₂, and WSe₂) with Fast Heterogeneous Electron Transfer: Application on Second-Generation Enzyme-Based Biosensor. *ACS applied materials & interfaces* **2017**, *9*, 40697–40706.

(26) Tan, S. M.; Sofer, Z.; Luxa, J.; Pumera, M. Aromatic-exfoliated transition metal dichalcogenides: Implications for inherent electrochemistry and hydrogen evolution. *ACS Catalysis* **2016**, *6*, 4594–4607.

(27) Li, Y.; Duerloo, K.-A. N.; Wauson, K.; Reed, E. J. Structural semiconductor-to-semimetal phase transition in two-dimensional materials induced by electrostatic gating. *Nature communications* **2016**, *7*, 10671.

(28) Sun, X.; Wang, Z.; Li, Z.; Fu, Y. Q. Origin of structural transformation in mono-and bi-layered molybdenum disulfide. *Scientific reports* **2016**, *6*, 26666.

(29) Gao, G.; Jiao, Y.; Ma, F.; Jiao, Y.; Waclawik, E.; Du, A. Charge mediated semiconducting-to-metallic phase transition in molybdenum disulfide monolayer and hydrogen evolution reaction in new 1T phase. *The Journal of Physical Chemistry C* **2015**, *119*, 13124–13128.

(30) Kresse, G.; Furthmüller, J. Efficiency of ab-initio total energy calculations for metals and semiconductors using a plane-wave basis set. *Computational Materials Science* **1996**, *6*, 15 – 50.

(31) Kresse, G.; Furthmüller, J. Efficient iterative schemes for ab initio total-energy calculations using a plane-wave basis set. *Phys. Rev. B* **1996**, *54*, 11169–11186.

(32) Kresse, G.; Joubert, D. From ultrasoft pseudopotentials to the projector augmented-wave method. *Phys. Rev. B* **1999**, *59*, 1758–1775.

(33) Klimeš, J. c. v.; Bowler, D. R.; Michaelides, A. Van der Waals density functionals applied to solids. *Phys. Rev. B* **2011**, *83*, 195131.

(34) Dion, M.; Rydberg, H.; Schröder, E.; Langreth, D. C.; Lundqvist, B. I. Van der Waals Density Functional for General Geometries. *Phys. Rev. Lett.* **2004**, *92*, 246401.

(35) Björkman, T. Testing several recent van der Waals density functionals for layered structures. *The Journal of chemical physics* **2014**, *141*, 074708.

(36) Patil, U.; Caffrey, N. M. Adsorption of common solvent molecules on graphene and MoS₂ from first-principles. *The Journal of Chemical Physics* **2018**, *149*, 94702.

(37) Henkelman, G.; Uberuaga, B. P.; Jónsson, H. A climbing image nudged elastic band method for finding saddle points and minimum energy paths. *The Journal of chemical physics* **2000**, *113*, 9901–9904.

(38) Henkelman, G.; Jónsson, H. Improved tangent estimate in the nudged elastic band method for finding minimum energy paths and saddle points. *The Journal of chemical physics* **2000**, *113*, 9978–9985.

(39) Gordon, R.; Yang, D.; Crozier, E.; Jiang, D.; Frindt, R. Structures of exfoliated single layers of WS₂, MoS₂, and MoSe₂ in aqueous suspension. *Physical Review B* **2002**, *65*, 125407.

(40) Heising, J.; Kanatzidis, M. G. Structure of restacked MoS₂ and WS₂ elucidated by electron crystallography. *Journal of the American Chemical Society* **1999**, *121*, 638–643.

(41) Wildervanck, J.; Jellinek, F. Preparation and crystallinity of molybdenum and tungsten sulfides. *Zeitschrift für anorganische und allgemeine Chemie* **1964**, *328*, 309–318.

(42) Schönfeld, B.; Huang, J.; Moss, S. Anisotropic mean-square displacements (MSD) in single-crystals of 2H-and 3R-MoS₂. *Acta Crystallographica Section B* **1983**, *39*, 404–407.

(43) Bronsema, K.; De Boer, J.; Jellinek, F. On the structure of molybdenum diselenide and disulfide. *Zeitschrift für anorganische und allgemeine Chemie* **1986**, *540*, 15–17.

(44) Schutte, W.; De Boer, J.; Jellinek, F. Crystal structures of tungsten disulfide and diselenide. *Journal of Solid State Chemistry* **1987**, *70*, 207–209.

(45) Dickinson, R. G.; Pauling, L. The crystal structure of molybdenite. *Journal of the American Chemical Society* **1923**, *45*, 1466–1471.

(46) Bell, R. E.; Herfert, R. E. Preparation and characterization of a new crystalline form of molybdenum disulfide. *Journal of the American Chemical Society* **1957**, *79*, 3351–3354.

(47) Podberezskaya, N.; Magarill, S.; Pervukhina, N.; Borisov, S. Crystal chemistry of dichalcogenides MX₂. *Journal of Structural Chemistry* **2001**, *42*, 654–681.

(48) Samadi, M.; Sarikhani, N.; Zirak, M.; Zhang, H.; Zhang, H.-L.; Moshfegh, A. Z. Group 6 transition metal dichalcogenide nanomaterials: synthesis, applications and future perspectives. *Nanoscale Horizons* **2018**, *3*, 90–204.

(49) Kumar, A.; Ahluwalia, P. Electronic structure of transition metal dichalcogenides monolayers 1H-MX₂ (M= Mo, W; X= S, Se, Te) from ab-initio theory: new direct band gap semiconductors. *The European Physical Journal B* **2012**, *85*, 186.

(50) Gusakova, J.; Wang, X.; Shiao, L. L.; Krivosheeva, A.; Shaposhnikov, V.; Borisenko, V.; Gusakov, V.; Tay, B. K. Electronic Properties of Bulk and Monolayer TMDs: Theoretical Study Within DFT Framework (GVJ-2e Method). *physica status solidi (a)* **2017**, *214*, 1700218.

(51) Liu, G.-B.; Shan, W.-Y.; Yao, Y.; Yao, W.; Xiao, D. Three-band tight-binding model for monolayers of group-VIB transition metal dichalcogenides. *Physical Review B* **2013**, *88*, 085433.

(52) García, Á. M.; del Corro, E.; Kalbac, M.; Frank, O. Tuning the electronic properties of monolayer and bilayer transition metal dichalcogenide compounds under direct out-of-plane compression. *Physical Chemistry Chemical Physics* **2017**, *19*, 13333–13340.

(53) Leng, K.; Chen, Z.; Zhao, X.; Tang, W.; Tian, B.; Nai, C. T.; Zhou, W.; Loh, K. P. Phase restructuring in transition metal dichalcogenides for highly stable energy storage. *ACS nano* **2016**, *10*, 9208–9215.

(54) Kwon, I. S.; Kwak, I. H.; Abbas, H. G.; Jung, G.; Lee, Y.; Park, J.; Yoo, S. J.; Kim, J.-G.; Kang, H. S. Intercalation of aromatic amine for the 2H–1T phase transition of MoS₂ by experiments and calculations. *Nanoscale* **2018**,

(55) Nasr Esfahani, D.; Leenaerts, O.; Sahin, H.; Parroens, B.; Peeters, F. Structural transitions in

monolayer MoS₂ by lithium adsorption. *The Journal of Physical Chemistry C* **2015**, *119*, 10602–10609.

(56) Kan, M.; Wang, J.; Li, X.; Zhang, S.; Li, Y.; Kawai, Y.; Sun, Q.; Jena, P. Structures and phase transition of a MoS₂ monolayer. *The Journal of Physical Chemistry C* **2014**, *118*, 1515–1522.

(57) Rasmussen, F. A.; Thygesen, K. S. Computational 2D materials database: electronic structure of transition-metal dichalcogenides and oxides. *The Journal of Physical Chemistry C* **2015**, *119*, 13169–13183.

(58) Zhuang, H. L.; Hennig, R. G. Computational search for single-layer transition-metal dichalcogenide photocatalysts. *The Journal of Physical Chemistry C* **2013**, *117*, 20440–20445.

(59) Liu, Y.; Wang, V.; Xia, M.; Zhang, S. First-principles study on structural, thermal, mechanical and dynamic stability of T'-MoS₂. *Journal of Physics: Condensed Matter* **2017**, *29*, 095702.

(60) Andreussi, O.; Marzari, N. Electrostatics of solvated systems in periodic boundary conditions. *Physical Review B* **2014**, *90*, 245101.

(61) Kim, M.-C.; Sim, E.; Burke, K. Communication: Avoiding unbound anions in density functional calculations. 2011.

(62) Topsakal, M.; Ciraci, S. Effects of static charging and exfoliation of layered crystals. *Physical Review B* **2012**, *85*, 045121.

(63) Topsakal, M.; Ciraci, S. Static charging of graphene and graphite slabs. *Applied Physics Letters* **2011**, *98*, 131908.

(64) Bal, K. M.; Neyts, E. C. Modelling molecular adsorption on charged or polarized surfaces: a critical flaw in common approaches. *Physical Chemistry Chemical Physics* **2018**, *20*, 8456–8459.

(65) Li, Q.; Yao, Z.; Wu, J.; Mitra, S.; Hao, S.; Sahu, T. S.; Li, Y.; Wolverton, C.; Dravid, V. P. Intermediate phases in sodium intercalation into MoS₂ nanosheets and their implications for sodium-ion batteries. *Nano Energy* **2017**, *38*, 342–349.

(66) Papageorgopoulos, C.; Jaegermann, W. Li intercalation across and along the van der Waals surfaces of MoS₂ (0001). *Surface science* **1995**, *338*, 83–93.

(67) Hong, J.; Pan, Y.; Hu, Z.; Lv, D.; Jin, C.; Ji, W.; Yuan, J.; Zhang, Z. Direct imaging of kinetic pathways of atomic diffusion in monolayer molybdenum disulfide. *Nano letters* **2017**, *17*, 3383–3390.

(68) Tang, W.; Sanville, E.; Henkelman, G. A grid-based Bader analysis algorithm without lattice bias. *Journal of Physics: Condensed Matter* **2009**, *21*, 084204.

(69) Enyashin, A. N.; Seifert, G. Density-functional study of Li_xMoS₂ intercalates (0 ≤ x ≤ 1). *Computational and Theoretical Chemistry* **2012**, *999*, 13–20.